Energy 261 (2022) 125171

Contents lists available at ScienceDirect

Energy

journal homepage: www.elsevier.com/locate/energy

A novel probabilistic power curve model to predict the power production and its uncertainty for a wind farm over complex terrain

Guo-Wei Qian [a,b], Takeshi Ishihara [b,*]

[a] School of Ocean Engineering and Technology, Sun Yat-sen University, Zhuhai 519082, China
[b] Department of Civil Engineering, School of Engineering, The University of Tokyo, 7-3-1, Hongo, Bunkyo-ku, Tokyo, Japan

ARTICLE INFO

Keywords:
Probabilistic power curve model
Uncertainty estimation
Power production of wind farm
Complex terrain

ABSTRACT

This study proposes a novel probabilistic power curve model for wind turbine and combines it with a hybrid wind farm model to quantify the accuracy and uncertainty of power prediction of wind farm over complex terrain with low computational cost. The proposed probabilistic power curve model for an active stall-regulated turbine is expressed by the beta distribution to estimate the uncertainty of power output at a certain wind speed. The predicted mean value and standard deviation of power output by the proposed model show favorable agreement with the measurement, while the conventional deterministic model cannot estimate the uncertainty of power output from wind turbines at all. The hybrid wind farm flow model is then presented, in which the effects of local terrain and surface roughness on the wind speed, wind direction and turbulence intensity are taken into account by the CFD simulation, and the wind turbine wakes are represented by an advanced wake model. The predicted wind speed and turbulence intensity show good agreement with those measured in a wind farm over complex terrain in the north of Japan. Finally, the proposed probabilistic power curve model is combined with the hybrid farm flow model to estimate the mean value and standard deviation of wind farm power production and is validated by the field measurement. The weighted mean absolute percentage error in mean value is reduced from 18.1% to 7.2% with consideration of wake effects and that in standard deviation is reduced from 100% to 15.6% by using the proposed probabilistic power curve model.

1. Introduction

Accurate prediction of wind farm power production is not only important for developers to identify potential energy, but also for grid operators to support the system scheduling and unit commitment. However, as outlined in the WindFarmer theory manual [1], the energy production calculation of a wind farm is always subject to three main areas of uncertainty: measurement uncertainty due to anemometry characteristics of devices at the reference site, wind condition variability due to the statistical fluctuation of wind resources over the historical period, and wind farm modelling uncertainty. The anemometry uncertainties can be estimated following the procedures defined by IEC 61400-12-1 [2], and the wind condition variability are usually evaluated through analysis of a long-term measurement data. In a wind farm modelling, the incident wind speeds at each turbine are firstly estimated with consideration of wind turbine wakes, topographic and site roughness effects, and then inputted to the power curve of the turbine to predict the power production for the whole wind farm. Thus, modelling uncertainties mainly arise from two aspects: wind speed prediction error in wake model and flow model over terrain, and power output error in wind turbine power curve (WTPC) model.

Many researches have been conducted to improve the accuracy of WTPC model. As summarized by Wang et al. [3], WTPC models can be classified into two main categories: deterministic model and probabilistic model. Deterministic models can be divided into discrete, curve fitting, and nonparametric methods. (1) The discrete method or so-called Bin method divides the entire wind speed range into several intervals with a bin of 0.5 m/s, and averaged pairs of wind speed and power in each bin are obtained by the procedures as defined in IEC 61400-12-1 (2005). The WTPC provided by the manufacture is normally presented in this way as well. (2) The curve fitting method use a set of piecewise or a single continuous mathematical expression to fit the relationship between wind speed and power, including linear equations [4], polynomial functions [5], and other S-shaped functions, e.g. Sigmoid function [6], and logistic functions [7,8]. (3) Nonparametric model does not have an explicit mathematical function but is

* Corresponding author.
E-mail addresses: qian@bridge.t.u-tokyo.ac.jp (G.-W. Qian), ishihara@bridge.t.u-tokyo.ac.jp (T. Ishihara).

https://doi.org/10.1016/j.energy.2022.125171
Received 30 June 2022; Accepted 13 August 2022
Available online 19 August 2022

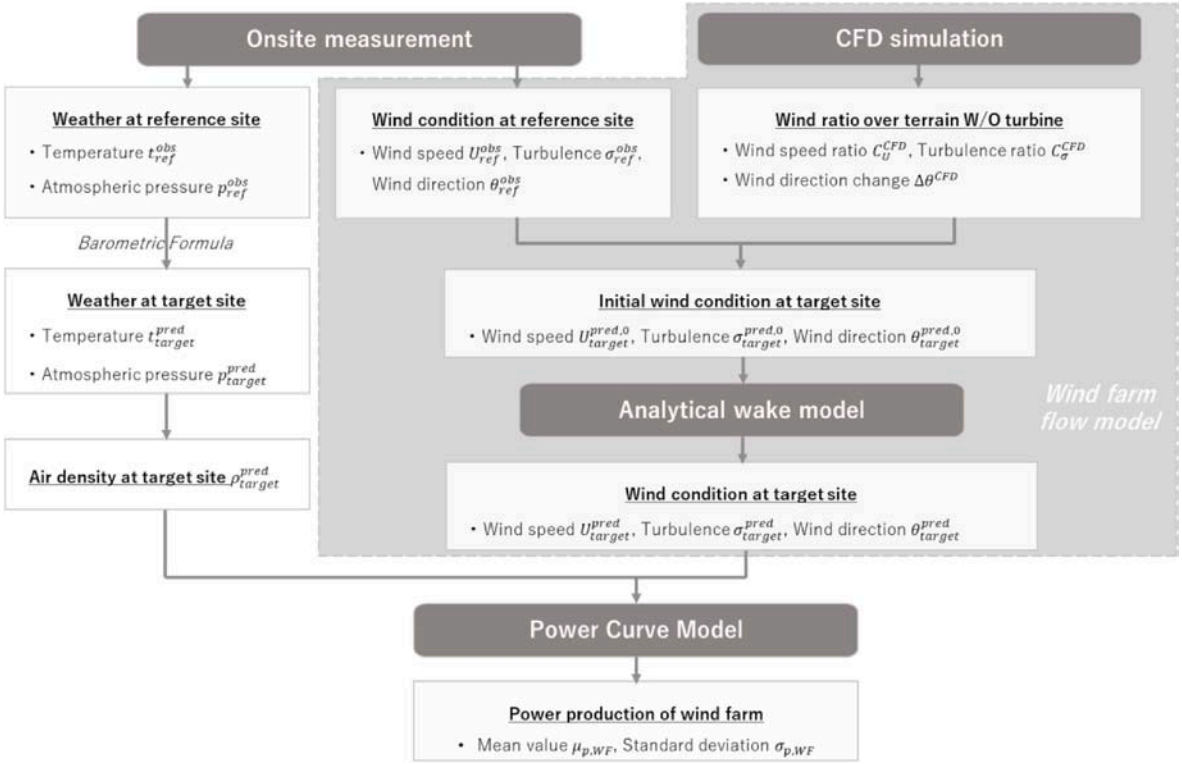

Fig. 1. Schematic of the on-site measurement-based power prediction for a wind farm over complex terrain.

constructed through undefined or virtual function with a data mining algorithm to approximate the relationship between wind condition and power output. Commonly used nonparametric methods include six categories: regression model [9,10], neural network [11], clustering method [12], k-nearest neighbor model (KNN) [13], adaptive neuro-fuzzy interference system (ANFIS) model [14] and copula model [15,16]. The deterministic model approximates the power with a specific one-to-one relationship, however, the actual wind turbine produces different powers even if the wind speed at the hub height is the same. This is due to the complex wind conditions (turbulence, air density, wind shear, etc.) and wind turbine operation conditions (rotor speed, pitch angle, aerodynamics of turbine blades, etc.).

In order to overcome the limitation of deterministic model, some researches have been shifting their attention to the probabilistic method to estimate the uncertainty of WTPC and to improve the reliability for the WTPC based wind farm power prediction. The probabilistic WTPC model is constructed with the assumption that at a particular wind speed, the corresponding wind power is considered as a random variable. It can be presented by a mean power with a standard deviation [17], a series of power curves by quantiles [18], percentiles [19], or upper and lower bounds under certain confidence levels [20]. The probabilistic WTPC model can also be divided to parametric type and nonparametric type based on the approach to describe the distribution of power. For the former one, the variation of power output within a wind speed bin was assumed to follow a normal distribution, where the standard deviation in each bin was assumed to be constant [21] or varied for the pitch-controlled wind turbine [17,19]. However, as pointed by Lange and Focken [22], the power prediction error in terms of the wind speed distribution for small and large wind speeds are strongly deformed to be non-Gaussian and no longer symmetric. It implies that the normal distribution is not properly to describe the uncertainty of power output for all wind speed region. Different from the parametric method which simulates the WTPC uncertainty by know distribution or computing statistical parameters, recently nonparametric methodologies, like neural networks, with no assumption on any known distribution or statistical properties are employed to build the probabilistic WTPC [18,20,23]. Nevertheless, these data-driven method needs a very careful process of data collection, clearing, training and verification, which takes higher computational cost and causes larger prediction error when these trained modules are used for different wind conditions and wind turbines compared to parametric model.

By utilizing a probabilistic WTPC model, Kwon [24] presented a framework to assess the uncertainty of AEP of a wind turbine based on a Monte-Carlo simulation, where the natural variability of wind conditions and error for prediction of long-term wind speed are also considered using probabilistic models. To sum up, most of the previous researches worked on the uncertainty estimation of power output for a single wind turbine, while very few works address that for a whole wind farm. To do this, in addition to the power curve model, a wind farm flow model including the layout wakes and topographical effects is necessary as well. Although FLORIS [25] can predict the wind speed and wind power in a wind farm over flat terrain, the topographic effects have not been incorporated yet. WindFarmer [1] is used for wind farm layout optimization over complex terrain with the modified PARK model, however, the multiple wake effects are not accurately considered as pointed by Qian and Ishihara [26].

Therefore, this study proposes a novel probabilistic model with two parameters for WTPC to quantify the uncertainty of power production of wind farm over complex terrain at low computational cost. Section 2 introduces the methodology, including the proposed probabilistic power curve model, a hybrid wind farm flow model, and the onsite measurements setup. In section 3, the proposed models for prediction of wind farm flow and power production are validated by the observed data. Conclusions are summarized in section 4.

2. Methodology

The framework developed in this study to predict the power production of wind farm over complex terrain is shown in Fig. 1. Section 2.1 elaborates the formulation of a novel probabilistic power curve model,

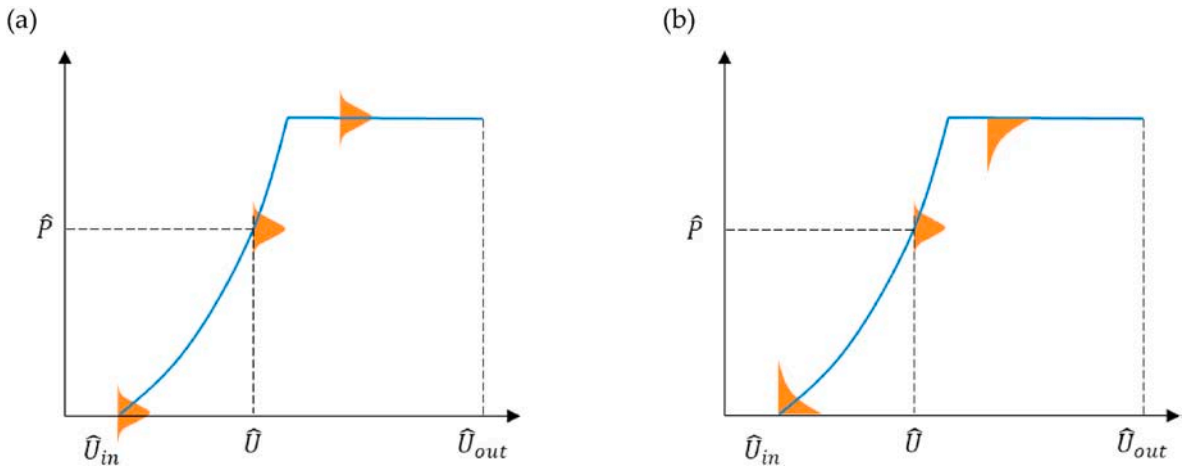

Fig. 2. Schematic of the probabilistic wind turbine power curve model: (a) normal distribution model and (b) beta distribution model.

which can estimate the expected power output with probability distribution. A hybrid wind farm flow model is then introduced in section 2.2, which involves numerical simulation of flow field over complex terrain without wind turbines and prediction of layout effects in the wind farm by an analytical wake model. The wind farm information including wind turbines and measurement device setups are described in section 2.3.

2.1. A novel probabilistic power curve model

As mentioned in Section 1, the existing probabilistic models mostly take the assumption that the power fluctuation follows a normal distribution which has a non-bounded symmetric bell-shape with respect to the mean value. However, since the power output is normally bounded with the low limit of zero and high limit of rated value, the power distribution will be asymmetrical near the cut in wind speed and rated wind speed, especially if the power is highly scatted [22]. In addition, when the wind speed is larger than rated one or lower than cut-in wind speed, the power distribution is more likely to be J-shaped or reverse-J-shaped as shown in Fig. 2. Instead of the normal density function, the beta density function is used to build a novel probabilistic WTPC model in this study since it can take a wide variety of different shapes including symmetrical or asymmetrical bell-shape, J-shape using only two parameters. The model is described as follows.

The Beta distribution is a family of continuous probability distributions defined in the interval [0, 1], thus, if the power output P is normalized by the rated power P_r, the normalized power output $\hat{P}$ at a certain wind speed is assumed to follow a beta distribution as follows.

$$\hat{P} = \frac{P}{P_r} \tag{1}$$

$$\hat{P} \sim \mathrm{Beta}(\alpha,\ \beta) \tag{2}$$

where α and β are two positive parameters which appear as exponents of the random variable and control the shape of the distribution. The probability density function (PDF) of the normalized power is expressed as follows:

$$f(\hat{P};\alpha,\ \beta) = \frac{\hat{P}^{\alpha-1}(1-\hat{P})}{\mathrm{B}(\alpha,\ \beta)} \tag{3}$$

where B is the beta function which is a normalization constant to ensure that the total probability is 1 and defined by the integral:

$$\mathrm{B}(\alpha,\ \beta) = \int_0^1 t^{\alpha-1}(1-t)^{\beta-1}dt \tag{4}$$

The mean value $\mu_{\hat{P}}$ and standard deviation $\sigma_{\hat{P}}$ of the normalized power at a certain wind speed can be theoretically obtained as

$$\mu_{\hat{P}} = \frac{\alpha}{\alpha+\beta} \tag{5}$$

$$\sigma_{\hat{P}} = \sqrt{\frac{\alpha\beta}{(\alpha+\beta)^2(\alpha+\beta+1)}} \tag{6}$$

If the mean value and the standard deviation of the power at each wind speed are available, the shape parameters of α and β can be directly derived as follows:

$$\alpha = \frac{\mu_{\hat{P}}^2 - \mu_{\hat{P}}^3}{\sigma_{\hat{P}}^2} - \mu_{\hat{P}} \tag{7}$$

$$\beta = \frac{\mu_{\hat{P}} - 2\mu_{\hat{P}}^2 + \mu_{\hat{P}}^3}{\sigma_{\hat{P}}^2} + \mu_{\hat{P}} - 1 \tag{8}$$

Since the above obtained α and β are discrete and may has uncertainty due to the limited amount of data at a certain bin of wind speed, in this study, they are modelled as exponential functions of wind speed as follows:

$$\alpha = m\exp[n_1(\hat{U} - \hat{U}_m)] \tag{9}$$

$$\beta = m\exp[n_2(\hat{U} - \hat{U}_m)] \tag{10}$$

where m and n are constants identified by the measurement data. The detailed explanations of curve fitting for the shape parameters α and β are described in section 3.1. $\hat{U}$ is the wind speed normalized by rated wind speed U_r and expressed as

$$\hat{U} = \frac{U}{U_r} \tag{11}$$

The shape of beta density function is expected to be symmetric ($\alpha = \beta$) at the normalized median wind speed $\hat{U}_m$, which is the midpoint between the cut-in wind speed U_{in} and the rated wind speed U_r as defined in the following equation:

$$\hat{U}_m = \frac{U_{in} + U_r}{2U_r} \tag{12}$$

The probabilistic WTPC model is implemented to predict the mean value and standard deviation of power output at a certain wind speed U as follows

$$\mu_P(U) = \mu_{\hat{P}}(U_n)\cdot P_r \tag{13}$$

Table 1
Summary of the Ishihara-Qian' wake model.

Wake model	Formulas	Parameters
Wake width	$\frac{\sigma}{D} = k^*\frac{x}{D} + \varepsilon^*$, $D_w = 4\sqrt{2\ln 2}\sigma$	$k^* = 0.11C_T'^{1.07}I_a^{0.20}$ $\varepsilon^* = 0.23C_T' - 0.25I_a^{0.17}$ $C_T' = C_T(U_h,\gamma)\cos\gamma,\ I_a \geq 0.03$
Velocity deficit	$\Delta U(x,y,z)/U_h = \frac{1}{\{a + b\cdot x/D + c(1+x/D)^{-2}\}^2}\cdot\exp\left(-\frac{r^2}{2\sigma^2}\right)$ $r = \sqrt{(y-y_d)^2 + (z-H)^2}$	$a = 0.93C_T'^{-0.75}I_a^{0.17}$ $b = 0.42C_T'0.6I_a^{0.2}$ $c = 0.15C_T' - 0.25I_a^{-0.7}$
Added turbulence	$\Delta\sigma_u(x,y,z)/U_h = \frac{1}{d + e\cdot x/D + f(1+x/D)^{-2}}\left\{k_1\exp\left(-\frac{(r-D/2)^2}{2\sigma^2}\right) + k_2\exp\left(-\frac{(r+D/2)^2}{2\sigma^2}\right)\right\} - \Delta I_a$ $\Delta I_a = \begin{cases} 0 & else \\ I_a\sin^2\left(\pi\frac{H-z}{D}\right)\cos^2\left(\pi\frac{y}{D}\right) & (0 \leq z < H, \lvert y\rvert \leq D) \end{cases}$	$d = 2.3C_T'^{-1.2}$, $e = 1.0I_a^{0.1}$ $f = 0.7C_T' - 3.2I_a^{-0.45}$ $k_1 = \begin{cases} cos^2(\pi/2\cdot(r/D-0.5)) & r/D \leq 0.5 \\ 1 & r/D > 0.5 \end{cases}$ $k_2 = \begin{cases} cos^2(\pi/2\cdot(r/D+0.5)) & r/D \leq 0.5 \\ 0 & r/D > 0.5 \end{cases}$
Deflection	$\frac{y_d(x)}{D} = \begin{cases} \theta_0\frac{x}{D} & (x \leq x_0) \\ \frac{\sqrt{C_T'}sin\gamma}{18.24k^*cos\gamma}ln\left\lvert\frac{(\sigma_0/D + 0.21\sqrt{C_T'})(\sigma/D - 0.21\sqrt{C_T'})}{(\sigma_0/D - 0.21\sqrt{C_T'})(\sigma/D + 0.21\sqrt{C_T'})}\right\rvert + \theta_0\frac{x_0}{D} & (x > x_0) \end{cases}$	$\theta_0 = \frac{0.3\gamma}{\cos\gamma}(1 - \sqrt{1 - C_T'})$ $\frac{\sigma_0}{D} = \sqrt{C_T'\left(\frac{sin\gamma}{44.4\theta_0 cos\gamma} + 0.042\right)}$ $\frac{x_0}{D} = \frac{\sigma_0/D - \varepsilon^*}{k^*}$

$$\sigma_P(U) = \sigma_{\hat{P}}(U_n)\cdot P_r \tag{14}$$

where U_n is a corrected 10-min mean wind speed to consider the effect of air density on the power curve following the approach in IEC 61400-12-1 (2005) as

$$U_n = U\left(\frac{\rho}{\rho_0}\right)^{1/3} \tag{15}$$

where ρ_0 is the standard air density (1.225 kg/m^3). The air density ρ (kg/m^3) at the turbine hub height is calculated using the ideal gas law, expressed as a function of temperature t (° C) and pressure p (Pa) as

$$\rho = \frac{p}{R(t + 273.15)} \tag{16}$$

where R is the gas constant for dry air (287.058 J/kgK). The atmospheric pressure p and temperature t at the turbine hub height are calculated based on the Barometric formula as follows

$$t_{target}^{pred} = t_{ref}^{obs} - \left(h_{target} - h_{ref}\right)L \tag{17}$$

$$p_{target}^{pred} = p_{ref}^{obs}\left[\frac{t_{target}^{pred} + 273.5}{t_{ref}^{obs} + 273.5}\right]^{5.257} \tag{18}$$

where h_{target} is the altitude of wind turbine hub height, L is the temperature lapse rate with the value of 0.0065 K/m, t_{ref}^{obs} and p_{ref}^{obs} are the onsite measured temperature and pressure at the reference site with the altitude of h_{ref}.

2.2. A hybrid wind farm flow model

A hybrid framework for onsite-measurement-based wind farm flow prediction over complex terrain is introduced by Qian and Ishihara [27]. The detailed procedures to set up the hybrid framework are illustrated in Fig. 1.

Firstly, based on the digital elevation model (DEM) and the surface roughness database (SRD), CFD simulations without turbines are performed for 16 sectors to provide a normalized wind field information. In this study, LES with Smagorinsky-Lill model in ANSYS Fluent 16.2 [28] is used to simulate the wind filed over complex terrain. The finite volume method (FVM) is applied for the discretization of the governing partial differential equations. The bounded central difference scheme is used for the interpolation of velocities. SIMPLE (semi-implicit pressure linked equations) algorithm is employed for solving the discretized equations. A second-order implicit scheme is adopted to approximate the time derivatives for unsteady term.

The wind speed ratio C_U^{CFD}, the turbulent standard deviation ratio C_σ^{CFD}, and the changes in wind direction $\Delta\theta^{CFD}$ between the target site and reference site are obtained and stored as functions of wind sector n as follows:

$$C_U^{CFD}(x,y,z,n) = \frac{U_{target}^{CFD}(x,y,z,n)}{U_{ref}^{CFD}\left(x_{ref},y_{ref},z_{ref},n\right)} \tag{19}$$

$$C_\sigma^{CFD}(x,y,z,n) = \frac{\sigma_{target}^{CFD}(x,y,z,n)}{\sigma_{ref}^{CFD}\left(x_{ref},y_{ref},z_{ref},n\right)} \tag{20}$$

$$\Delta\theta^{CFD}(x,y,z,n) = \theta_{target}^{CFD}(x,y,z,n) - \theta_{ref}^{CFD}\left(x_{ref},y_{ref},z_{ref},n\right) \tag{21}$$

Secondly, the on-site measurement provides the measured wind speed $U_{\mathrm{ref}}^{\mathrm{obs}}$, turbulence standard deviation σ_{ref}^{obs}, and wind direction $\theta_{ref}^{\mathrm{obs}}$ at the reference height where the observation is not affected by the wind turbine wakes in the wind farm.

Subsequently, the wind field without the effects of turbines including wind speeds $U_{\mathrm{target}}^{\mathrm{pred,0}}(x,y,z)$, turbulence standard deviation $\sigma_{\mathrm{target}}^{\mathrm{pred,0}}(x,y,z)$ and wind direction $\theta_{\mathrm{target}}^{\mathrm{pred,0}}(x,y,z)$ at the target site are estimated following the approach by Misu and Ishihara [29] with the expressions as:

$$U_{target}^{pred,0}(x,y,z) = U_{ref}^{obs}\cdot C_U^{CFD}\left(x,y,z,\theta_{ref}^{obs}\right) \tag{22}$$

$$\sigma_{target}^{pred,0}(x,y,z) = \sigma_{ref}^{obs}\cdot C_\sigma^{CFD}\left(x,y,z,\theta_{ref}^{obs}\right) \tag{23}$$

$$\theta_{target}^{pred,0}(x,y,z) = \theta_{ref}^{obs} + \cdot\theta_{CFD}\left(x,y,z,\theta_{ref}^{obs}\right) \tag{24}$$

where $C_U^{CFD}(x,y,z,\theta_{ref}^{obs})$, $C_\sigma^{CFD}(x,y,z,\theta_{ref}^{obs})$ and $\Delta\theta^{CFD}(x,y,z,\theta_{ref}^{obs})$ are obtained by a linear interpolation on the stored data set as:

$$C_U^{\mathrm{CFD}}\left(\theta_{ref}^{obs}\right) = C_U^{CFD}(n) + a\left(C_U^{CFD}(n+1) - C_U^{CFD}(n)\right) \tag{25}$$

$$C_\sigma^{CFD}\left(\theta_{ref}^{\mathrm{obs}}\right) = C_\sigma^{CFD}(n) + a\left(C_\sigma^{CFD}(n+1) - C_\sigma^{CFD}(n)\right) \tag{26}$$

$$\Delta\theta^{CFD}\left(\theta_{ref}^{obs}\right) = \Delta\theta^{CFD}(n) + a\left(\Delta\theta^{CFD}(n+1) - \Delta\theta^{CFD}(n)\right) \tag{27}$$

Fig. 3. Test site in the Tomamae wind farm: (a) location of Tomamae; (b) aerial picture of wind farm; (c) wind turbine and its dimensions; (d) layout of the wind farm and measurement where the white open circles denote the location of each wind turbine, the red square and the blue triangles indicate the position of LiDAR and Met-masts (No.1, No.2 and No.3 from north to south) respectively.

where a is a proportional coefficient expressed by

$$a = \frac{\theta_{ref}^{\text{obs}} - \theta_{ref}^{CFD}(n)}{\theta_{ref}^{CFD}(n+1) - \theta_{ref}^{CFD}(n)} \tag{28}$$

n and $n+1$ denote the two adjacent wind sectors determined by the measured wind direction at reference site as

$$\theta_{ref}^{\text{obs}} \in \left(\theta_{ref}^{CFD}(n), \theta_{ref}^{CFD}(n+1)\right) \tag{29}$$

where $\theta_{ref}^{CFD}(n)$ and $\theta_{ref}^{CFD}(n+1)$ are wind directions obtained by CFD simulation for inlet flow direction sectors n and $n+1$ at the reference site.

After obtaining the initial wind condition at each turbine location, wind turbine wake effects need to be evaluated. Since the wind turbine wake is significantly affected by the local variation of wind speed, wind direction and turbulence induced by terrain, an attention needs to be paid to the choice of wake model. The Gaussian-based analytical wake model proposed by Refs. [30,31], noted as Ishihara-Qian model, which provides a three-dimensional wake characteristic including wake width, velocity deficit, added turbulence, as well as wake deflection caused by yaw or inclination offset. Recently, the Ishihara-Qian model are extended for multiple wake modelling, which shows good agreement with the power obtained from numerical simulations and field measurements in wind farms [26]. Based on the above considerations, the Ishihara-Qian model is utilized in this study for wind farm flow modelling. The detailed formula and parameters of wake model are summarized in Table 1, where the rotor onset wind speed $U_{h,i}$ and turbulence intensity $I_{a,i}$ will be used for multiple wake prediction to replace the U_h and I_a of ambient wind condition at the hub height.

Wind turbines over a terrain generally experience a non-uniform inflow due to the terrain effects and wakes from upstream turbines as well. Hence, the equivalent wind speed $U_{h,i}$ and turbulence intensity $I_{a,i}$ on the rotor, i.e., the rotor onset wind speed and turbulence intensity are firstly evaluated. As shown in Eqs. (28) and (29), the rotor onset $U_{h,i}$ is calculated by directly performing a geometric averaging of wind speed U over the rotor, while rotor onset $I_{a,i}$ is calculated by the root mean of squares of streamwise turbulence standard deviation σ_u over the rotor divided by the rotor onset wind speed $U_{h,i}$. To consider the wake interactions in wind farm, the wake superposition approach proposed by Qian and Ishihara [26] are applied here as well.

$$U_{h,i} = \frac{1}{A}\int_{rotor} U(x_i, y, z)dA \tag{30}$$

$$I_{a,i} = \frac{1}{AU_{h,i}}\sqrt{\int_{rotor} \sigma_u^2(x_i, y, z)dA} \tag{31}$$

Table 2
Specification of Bonus BS54/1000 wind turbine.

Parameter	Value
Rated capacity P_r	1000 kW
Hub height H	45 m
Rotor diameter D	54.2 m
Cut-in wind speed U_{in}	3 m/s
Cut-out wind speed U_{out}	25 m/s
Rated wind speed U_r	15 m/s
Rotor speed	Fixed speed, 14 rpm/21 rpm
Power control	Active stall-regulated

where x_i denotes the streamwise location of turbine, and A is the area of the rotor.

Finally, by superposing wake effects onto the pre-computed initial flow field, the wind conditions at the target sites are obtained as:

$$U_{target}^{pred}(x,y,z) = U_{target}^{pred,0}(x,y,z) - \Delta U(x,y,z) \tag{32}$$

$$I_{target}^{pred}(x,y,z) = \frac{\sqrt{\sigma_{target}^{pred,0}(x,y,z)^2 + \Delta\sigma(x,y,z)^2}}{U_{target}^{pred}(x,y,z)} \tag{33}$$

$$\theta_{target}^{pred}(x,y,z) = \theta_{target}^{pred,0}(x,y,z) \tag{34}$$

where ΔU and $\Delta\sigma$ are the turbine wake induced velocity deficit and added turbulence standard deviation calculated by using the analytical model as shown in Table 1. The parameters in the wake model are described in detail in Refs. [30,31].

2.3. Description of wind farm and measurement data

In this study, a field measurement campaign is conducted at the Tomamae wind farm, located in Hokkaido facing the Japan Sea. The prominent topographic feature of this site is a steep escarpment along the west coast as shown in Fig. 3. In addition, the east onshore site is mainly characterized by the ranch, farmland, grass, and nearby

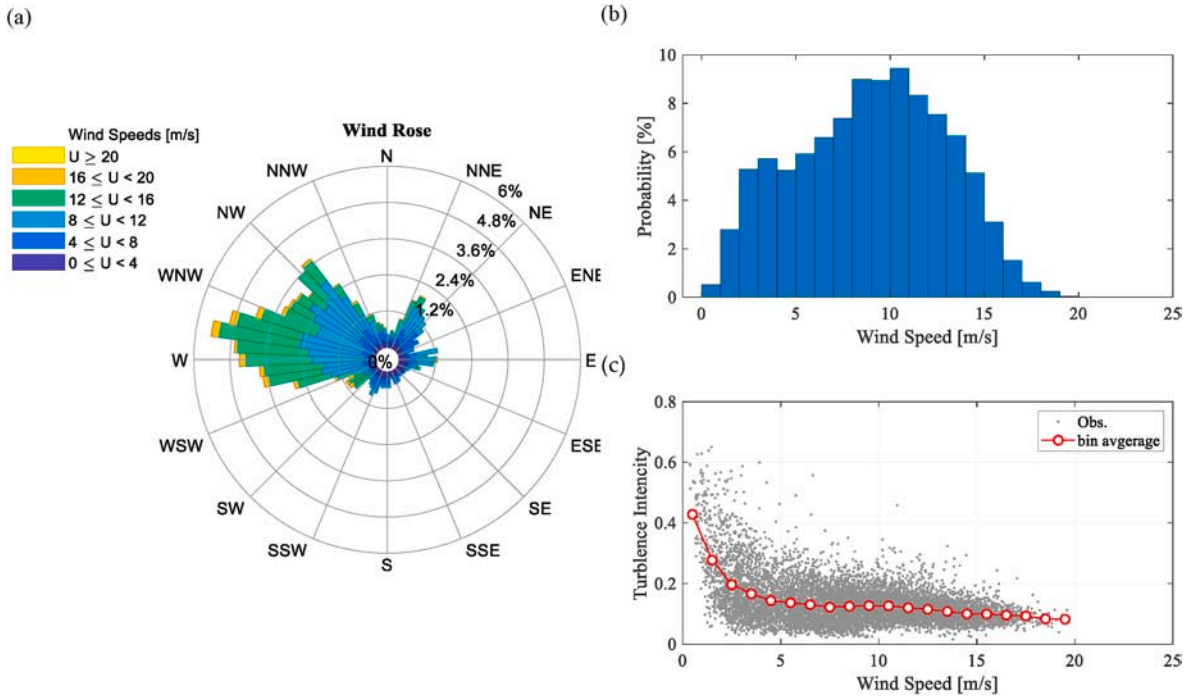

Fig. 4. Reference wind condition at the height of 120 m measured by the Doppler LiDAR from November 2015 to January 2016: (a) wind rose, (b) frequency distribution of wind speeds and (c) distribution of turbulence intensity versus wind speed.

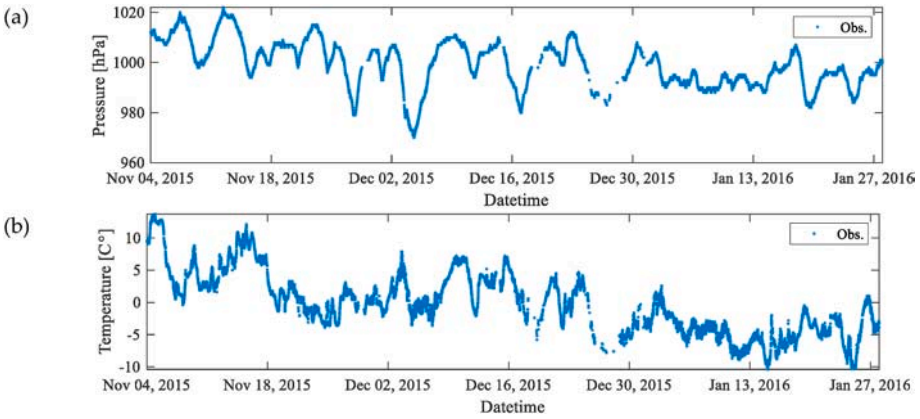

Fig. 5. Time series of 10-minutue averaged (a) atmospheric pressure and (b) temperature measured at the height of 75 m by Met-mast No.1.

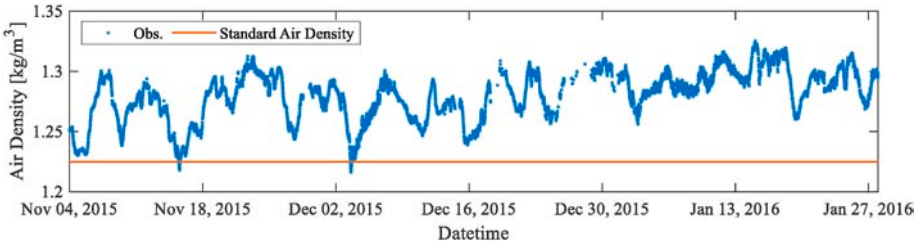

Fig. 6. Time series of 10-minutue averaged air density at wind turbine hub height at the location of Met-mast No.1. The orange line denotes the value of standard air density.

Table 3
Data cleaning criterion for SCADA data analysis.

Filter	Criterion
(1) Wind speed (m/ s)	$U > 0$
(2) Rotor speed (rpm)	$\Omega > 0$
(3) Power (kW)	$P \geq 1$
(4) Power in each wind speed bin (kW)	$\lvert P - m_P \rvert \leq 3\ \sigma_P$

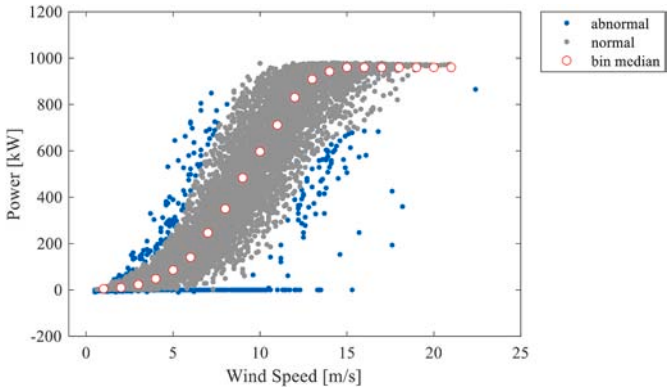

Fig. 7. Scatter plots of power versus wind speed with the data cleaning criteria for WT1.

buildings and forests, which adds to the complexity of the land surface roughness. Comprehensive measurement campaigns were carried out successively in the Tomamae wind farm, including a ground-based vertical profile LIDAR from November 2015 to January 2016 as described in Qian and Ishihara [27]; three Met-masts and Supervisory Control and Data Acquisition (SCADA) for each wind turbine from November 2015 to November 2017. The Mat-mast is a lattice tower equipped with anemometers measuring the wind speed between heights 10 m and 80 m at an interval of 10 m, wind vans and sensors measuring the wind direction, atmospheric pressure, and temperature at height 75 m. The statistical data in every 10 min were recorded in the measurement system. The wind farm includes 19 Bonus 1 MW wind turbines (WT1∼10, WT12∼20) and one Unison 2 MW turbine (WT11) which is located on the east site of WT4. The Bonus 1 MW is an active stall-regulated turbine with a rotor diameter of 54.2 m and a hub height of 45.0 m, and its specification are summarized in Table 2.

The Doppler LiDAR is used to measure the wind direction and wind speed between the height 40 m and 120 m at an interval of 20 m. Since the wind speed and wind direction are not affected by wind turbine wakes at the height of 120 m, they are taken as the reference wind condition for the wind farm flow prediction. The wind rose is shown in Fig. 4a, in which wind sector width is set to 5°, and the west is the prevailing wind direction. The wind speed distribution is illustrated in Fig. 4b. The turbulence intensity versus wind speed with bin averaged values are also shown in Fig. 4c. It is found that the wind turbines at this site are operated under a relative high level of turbulence intensity.

The atmospheric pressure and temperature measured at the height 75 m of Met-mast-1 are plotted in Fig. 5, and the air density at the hub height calculated based on Eq. (11) are shown in Fig. 6. It can be seen that the actual air density is larger than the standard value due to the low temperature during the winter season in the north of Japan.

3. Results and discussion

The characteristics of power distribution of a representative turbine in the wind farm is analyzed and the proposed probabilistic power curve model is validated in section 3.1. The numerical setup for the CFD simulation is then described in section 3.2, and the accuracy of the hybrid wind farm flow model is validated by comparing the predicted and measured wind field. Finally, the power of the wind farm and its uncertainty is predicted and validated in section 3.3.

3.1. Validation of proposed probabilistic power curve model

In general, the power curves of stall-regulated wind turbines with fixed speeds show larger scatter comparing those of pitch-regulated wind turbine with variable speeds as shown in Burton et al. [32]. It is because that the power coefficients change with the wind speed and turbulence intensity which results in the uncertainty of power output as pointed out by Aliferis et al. [33], while the power outputs of the pitch regulated wind turbine with variable speeds are controlled by the rotational speed and pitch angle decreasing the sensitivity to the turbulent inflow. In this study, an active stall-regulated wind turbine with fixed speeds in the Tomamae wind farm is selected to build the probabilistic power curve model and the rest of the wind turbines are used to validate the proposed model.

Wind turbine operational data usually has unreasonable data due to some abnormal situations including blackout, component failures, errors from measurement, curtailment, and maintenance, etc. These data cannot reflect the actual characteristics of the wind turbine, therefore the raw measurement data have to be cleaned out from abnormal operation based on a certain filtering criterion. Various filters for outlier detections in the WTPC have been applied in the existing research [3]. In this study, the data filtering conditions are shown in the following Table 3. The data cleaning is processed with the following two steps: Firstly, Filters (1)–(3) are practical yet straightforward SCADA data-based process, where positive power values, wind speed and rotor speed are identified. However, it is noted that the resulting SCADA data will not be entirely free from errors due to the irregular wind and operation conditions, such as unsteady wind conditions or unexpected stops. Thus, Filter (4) is then performed based on the Criterion (4). These abnormal situations are modelled separately as shown in WindFarmer theory manual (2014).

The wind speed range is firstly divided into several bins with interval of 1 m/s. For each bin, the median value m_P and the standard deviation for power output is calculated σ_P. It is noted that the center of each bin is represented by the median values of power instead of mean value so that the calculation is not biased by a few outliers [34,35], especially for the above rated region. In each wind speed bin, the power output that are

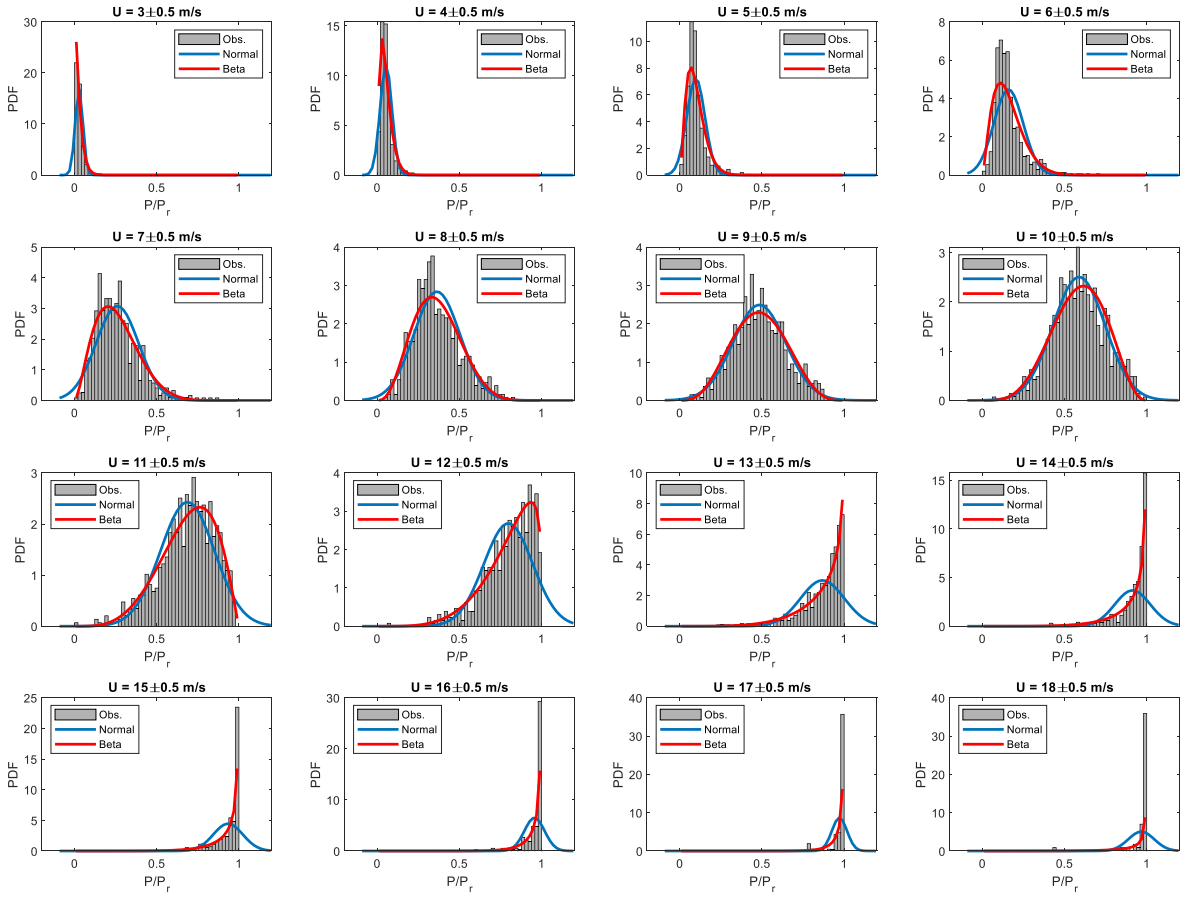

Fig. 8. Probability density distribution of power outputs within each wind speed bin for WT1.

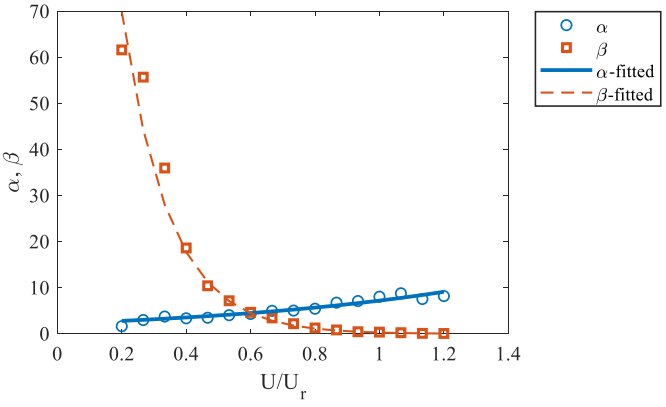

Fig. 9. Variation of shape parameters α and β with the normalized wind speed for WT1.

outside of $\pm 3\sigma_P$ are marked as outliers and are discarded. Fig. 7 shows an example of applying the data filtering for WT1, where the normal data and abnormal data are plotted by gray points and blue points, respectively. The median values in each bin are plotted in red open circles. Note that the bin median value at the above rated wind speed region is found to be $P_r = 970$ kW, which is used in the power curve modelling. Gray points in Fig. 7 are the cleaned data from WT1 and it is clear to see that the power is highly scattered with a wide band. This justifies the need to develop a probabilistic power curve model rather than a deterministic model.

The practical distribution of power points within each wind speed bin from 3 m/s to 18 m/s for WT1 are analyzed and shown in Fig. 8, where all the power data are normalized by the rated power. At the cut-in wind speed region, the distribution presents a reverse J-shape. Then, it becomes to a positively skewed bell-shape with right tail and the mode position increases with the increasing wind speed. When the wind speed increases to 9 m/s which is the midpoint between $U_{in} = 3m/s$ and $U_r = 15m/s$, the distribution displays a nearly symmetric bell shape. On the other hand, the shape of distribution gradually changes to negative skewed and left-tailed, which finally develops a J-shape. For each wind speed bin, the mean value and standard deviation of power are calculated and the shape parameters (α, β) of beta density function are then obtained by Eq. (7) and Eq. (8). The calculated (α, β) are then used to formulate the PDF for each bin of wind speed, which are plotted in red lines in Fig. 8. In addition, the PDF of normal distribution based on the calculated mean value and standard deviation are also plotted with blue dashed lines for comparison. The beta density function can favorably match the power distribution in any wind speed bin, however the normal density function cannot capture the uncertainty of power output in low wind speed region, as well as near and above rated wind speed region.

The shape parameter (α, β) of beta density function in each wind speed bin for WT1 are shown in Fig. 9, where the wind speed is normalized by U_r. It can be seen that, α and β are monotonically increasing and decreasing as wind speed increases, respectively, and they are approximately equal at the normalized median wind speed $\widehat{U}_m = 0.6$. Based on the proposed equation for α and β (see Eq. (9) and Eq. (10)), the fitted curves for them are obtained and favorably capture the values for different wind speed. The fitted constants in the shape parameter equations are $m = 4.51$, $n_1 = 1.18$, and $n_2 = -6.85$, which are applied for other turbines in the Tomamae wind farm to validate the accuracy of proposed power curve model.

The predicted power outputs of WT3 are compared with the

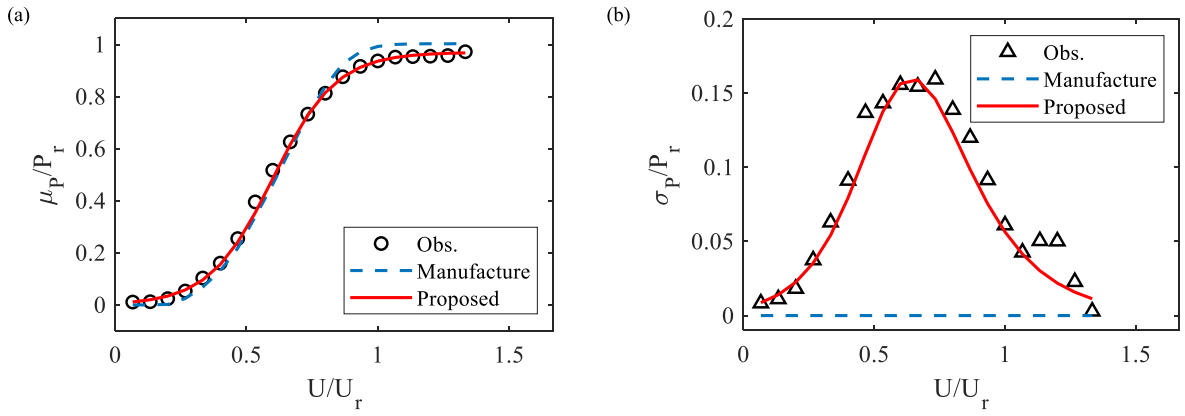

Fig. 10. Comparison of measured and predicted power outputs for WT3: (a) mean values, (b) standard deviations. The power outputs are normalized by the rated power of wind turbine P_r, and the wind speeds are normalized by the rated wind speed U_r.

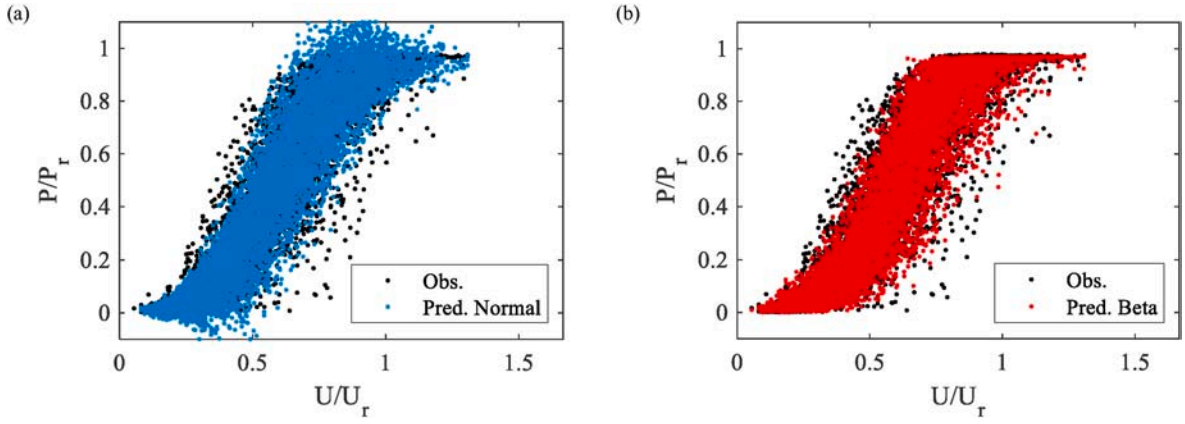

Fig. 11. Comparison of measured and predicted power outputs by (a) normal distribution and (b) beta distribution for WT3. The power outputs are normalized by the rated power of wind turbine P_r, and the wind speeds are normalized by the rated wind speed U_r.

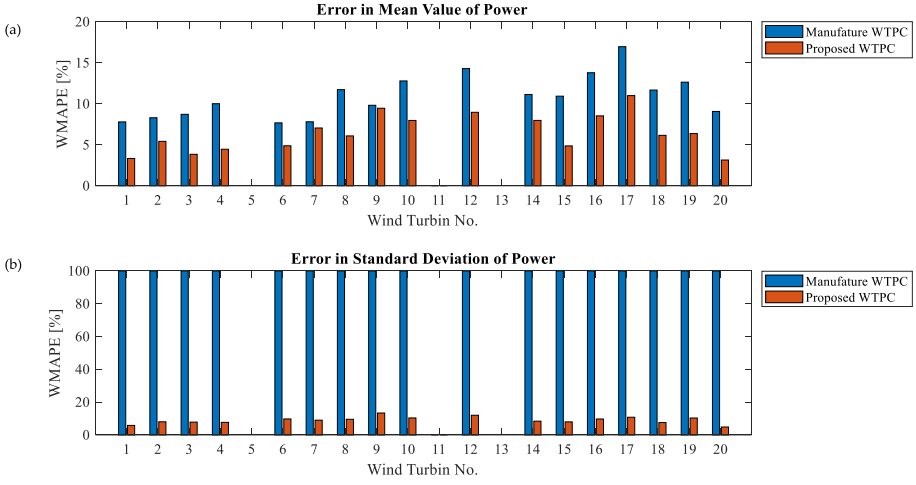

Fig. 12. Weighted mean absolute percentage errors in (a) mean value and (b) standard deviation of power output for each wind turbine.

measurements and are shown in Fig. 10. The mean value and standard deviation for each wind speed bin are firstly estimated by using Eq. (5) and Eq. (6) and compared with those obtained from the measured data as shown in Fig. 10a and b, where the predicted mean value and standard deviation of power output by the proposed probabilistic WTPC show good agreement with those from the measurement. However, the predicted mean values by the manufacture WTPC show slight overestimations in the higher wind speed region and the predicted standard deviation depicts significant underestimation. In addition, Fig. 11 presents the scatter plot of power outputs of WT3. The red dots randomly generated based on the beta density function in Fig. 11b can well reproduce the highly scattered data from measurement as shown in the black dots, while the normal distribution will generate negative values at low wind speed region and values higher than rated power

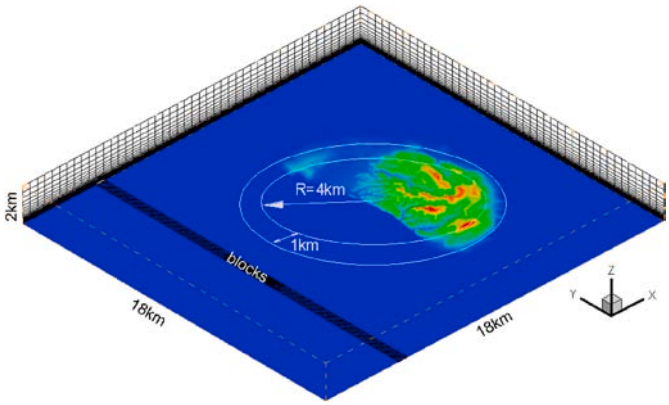

Fig. 13. Configuration of computational domain with terrain topography.

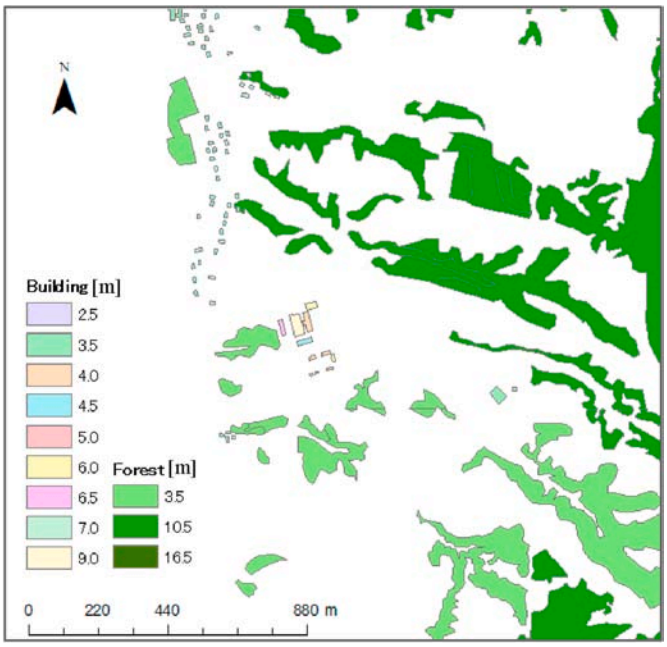

Fig. 14. Digital map of buildings and forests in the wind farm. The values of different legend represent the height of canopies.

near rated wind speed as shown by the blue dots in Fig. 11a.

In order to evaluate the errors in the predicted mean values and standard deviation of power output, the weighted mean absolute percentage error (WMAPE) is introduced as follows

$$\mathrm{WMAPE} = \frac{\sum_{i=1}^{N} f_i \left| x_i^{pred} - x_i^{obs} \right|}{\sum_{i=1}^{N} f_i x_i^{obs}} \tag{35}$$

where the x_i^{pred} and x_i^{obs} are the predicted and observed value in a certain wind speed bin i, respectively, and f_i denotes the occurrence of the hub height wind speed in the bin i, and N is the number of bins. The WMAPE in mean value and standard deviation of power for each wind turbine are summarized in Fig. 12a and Fig. 12b, respectively. Since the anemometer of WT5 and WT13 were in failure during the campaign and WT11 is a different type of turbine, they are not included in Fig. 12. The proposed probabilistic WTPC based on WT1 can significantly reduce the prediction errors for all the other turbines. The averaged WMAPE for the mean value decreases from 10.9% to 6.5% and that for the standard deviation decreases from 100% to 9%, respectively.

3.2. Prediction of wind farm flow over complex terrain and its validation

Firstly, the numerical setting for CFD simulation of wind flow over complex terrain without turbines are described. The general numerical simulation settings including critical mesh size and fluid conditions in this study are exactly identical to those in Qian and Ishihara [27]. As shown in Fig. 13, a numerical wind tunnel is built by the dimensions of 18km × 18km × 2 km in streamwise, spanwise and vertical directions with a scale of 1:2000. The height of domain is determined by limiting the blockage ratio to a specified value of 5%. Considering the average elevation in the site is lower than 100 m, 2 km is adopted as the calculation domain height. In the inflow generation zone, roughness blocks are placed 7 km upstream from the origin, where the neutrally stratified atmospheric boundary layer in the ocean side was simulated with the mean velocity profile following the power law of $\alpha = 0.1$. For the land side, the boundary layer would be automatically developed through the surrounding terrain and vegetations within the considered region. The location of WT12 is set as the origin of the computational domain.

The topography model with a scale of 1:2000 and a radius of 4 km is generated based on the digital elevation model (DEM), as shown in Fig. 13. For the sake of reducing calculation cost as well as keep prediction accuracy, a hybrid grid system is designed as presented in Qian and Ishihara [27]. The DEM database used in this research is provided by the Geospatial Information Authority of Japan [36] in raster format,

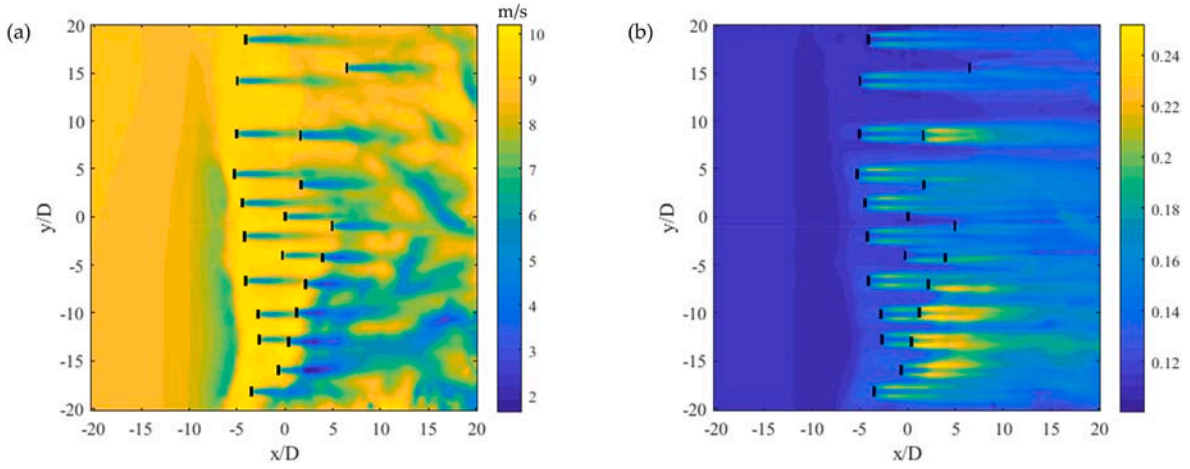

Fig. 15. Horizontal contour of wind speed at the hub height of wind turbine extracted from the simulated wind farm flow field: (a) mean wind speed and (b) turbulence intensity. The distances are normalized by the rotor diameter of wind turbine.

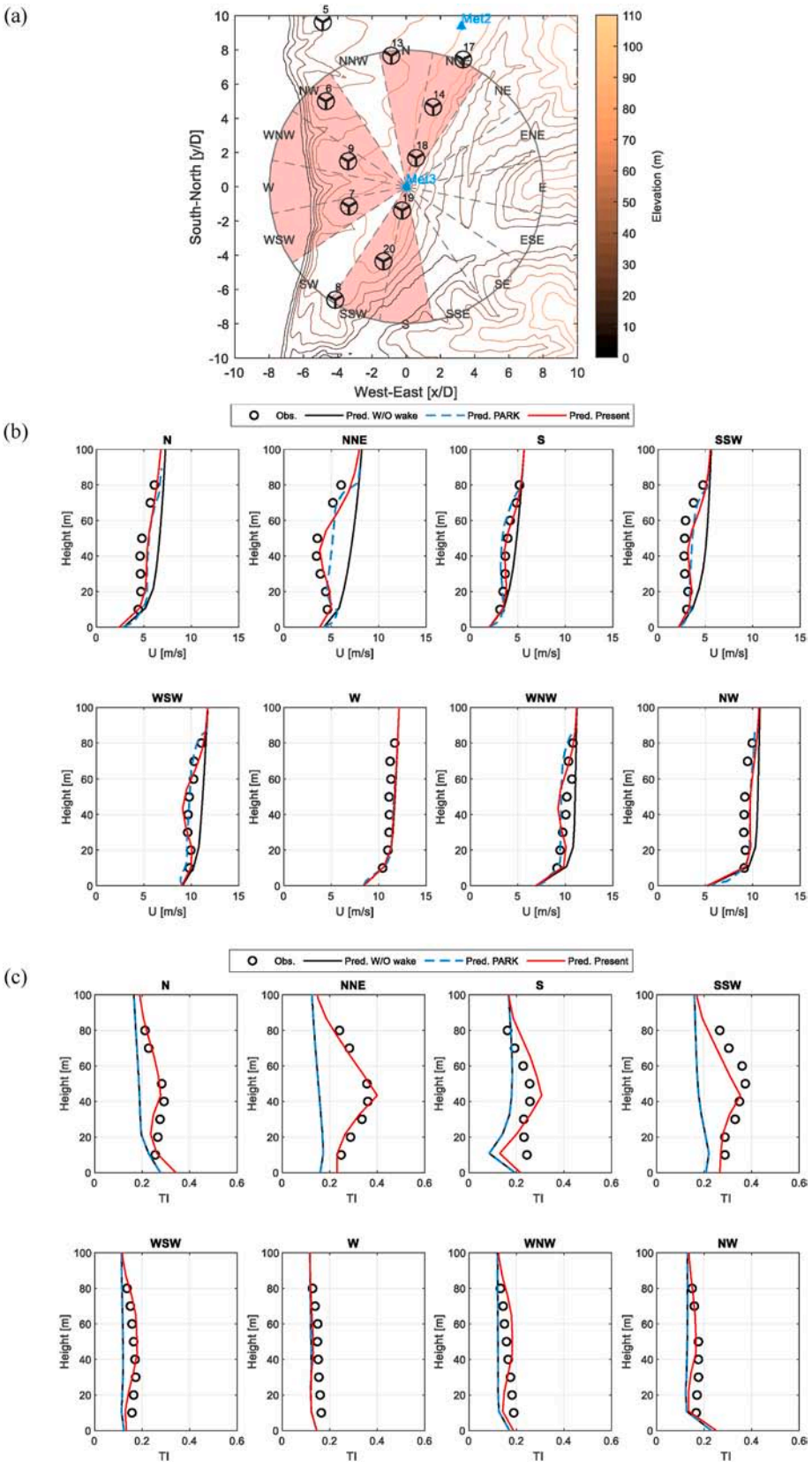

Fig. 16. Wind conditions at Met-mast No. 3: (a) Layout of Met-mast No.3 and its surrounding wind turbines. Comparison between predicted and measured (b) mean wind speed and (c) turbulence intensity at the location of Met-mast No.3 in the several typical wind directions.

which describes the topography in Japan with an available minimum resolution of 10 m × 10 m. The outer ring with width of 1 km is used to smooth the surrounding terrain. Since the buildings and forest are dominant surface roughness conditions and strongly affect the flow fields, the canopy model described by Ishihara et al. [37] are utilized to simulate the ground roughness effects. The distribution of the vegetation

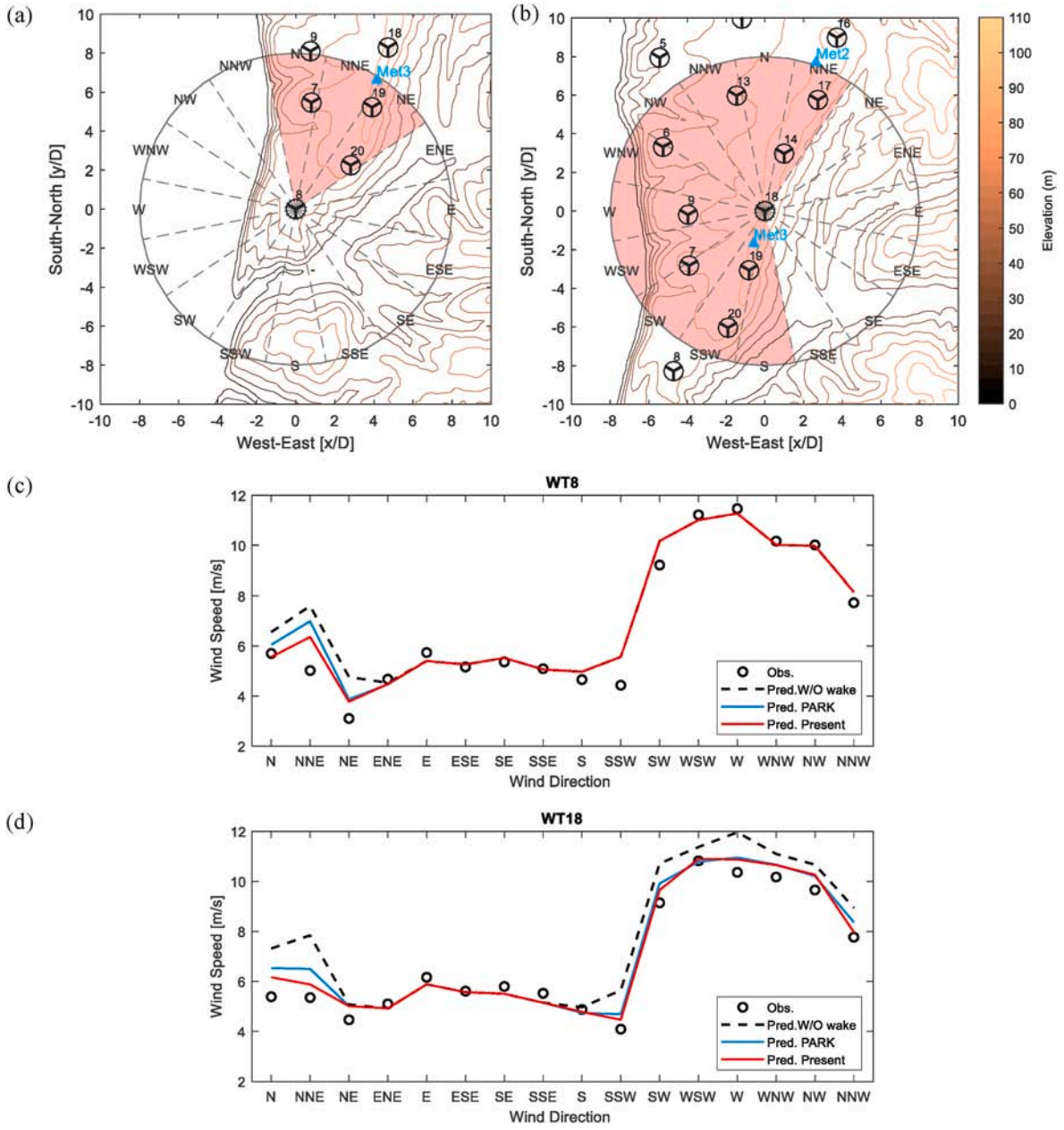

Fig. 17. Wind condition at WT8 and WT18: (a) and (b) Local layout of the target turbine and its surrounding turbines. Pink sectors denote the wind directions in which the target turbine is affected by wakes; Distribution of mean wind speed at the hub height in different wind directions for (c) WT8 and (d) WT18.

and buildings are obtained from the database provided by the Ministry of Land, Infrastructure, Transport and Tourism [38] and then locally modified based on the Google Earth. The height of buildings and different type of tress are identified via Google street view with photographical measurement [37]. The generated digital map of buildings and tress are shown in Fig. 14.

A stress-free condition ($\partial u/\partial n = 0$, $\partial v/\partial n = 0$, $w = 0$) is used at the top of the domain and a symmetry condition ($\partial u/\partial n = 0$, $\partial w/\partial n = 0$, $v = 0$) at the two sides. Uniform flow with a speed of 10 m/s is set at the inlet ($p = 0, u = 10$ m/s, $v = 0$, $w = 0$). At the end of the numerical wind tunnel, the outflow condition is applied ($\partial p/\partial n = 0$, $\partial u/\partial n = 0$, $\partial v/\partial n = 0$, $\partial w/\partial n = 0$). The wall-stress boundary condition is imposed at the ground surface, where the wall shear stresses are calculated following the log law of wall with roughness. The roughness length values for different areas are determined based on the land-use database provided by MLIT [38], while for those areas which are covered by canopy model, roughness length is modified to z0 = 0.01 m as shown in Ishihara et al. [39].

Once the normalized wind flow field at different wind direction are obtained by the CFD simulation, the flow field is then modified by using the wind farm model as presented in section 2.2, where the wind condition measured at 120 m by the LiDAR is used as the input. Fig. 15 shows an example of predicted wind speed and turbulence intensity at the hub height of the wind farm at a certain time step with incoming wind direction of W and wind speed of 10 m/s. There is a clear speed up at the east coastline where is characterized by an escarpment. The wind speed deficit and added turbulence intensity induced by the wind turbines are captured as well, which are calculated by the Ishihara-Qian wake model. One wind turbine, WT-Jpower, located at the east site of WT1 in the nearby wind farm is also included in the simulation.

To validate the hybrid wind farm flow model, the predicted wind conditions at several target sites are compared with those obtained from the measurement. Firstly, the predicted and measured mean wind speed and turbulence intensity at the site of Met-mast No. 3 are presented in

Fig. 16. Eight wind sectors affected by wind turbine wakes are filled with pink color as shown in Fig. 16a, and the vertical profiles of mean wind speed and turbulence intensity are illustrated in Fig. 16b and c, respectively. The open circles denote the measurement data, and the predicted results with and without wake effects are plotted by red and black solid lines, respectively. The results predicted by the modified PARK model in WindFarmer [1] are also plotted by blue dashed lines for comparison. The wind speed and turbulence intensity predicted by the present wind farm flow model are in good agreement with the measurement. For wind sectors where there is only one wind turbines in the upstream, the modified PARK model can provide good prediction as well, however, it underestimates the velocity deficit when the Met Mast 3 is affected by a couple of turbines, such as sector of NNE in Fig. 16a. The modified PARK model does not consider the turbine induced turbulence, thus it underestimates the turbulence intensity for all directions as shown in Fig. 16b.

Secondly, the mean wind speeds at two selected wind turbines are also shown in Fig. 17. Similarly, the local layout of target turbine and its surrounding turbines are shown in Figs. 17a and b for WT8 and WT18, respectively, where the wind sectors filled with pink color display the wind sectors that are affected by wind turbine wakes. From Fig. 17c and d, it can be seen that, in the wind direction without turbines in the upstream, the wind speeds predicted by CFD simulation agree well with those measured by the nacelle anemometer. In addition, for those wind sectors affected by the upstream turbines, the wind speed distribution is well reproduced by considering the wake effects through the Ishihara-Qian wake model. However, the modified PARK model overestimates the wind speed in the direction of N and NNE for WT8, and the direction of N, NNE, NNW for WT18.

3.3. Wind farm power prediction and uncertainty estimation

To predict the wind farm power production, the array efficiency which is dependent on the multiple wind turbine wake effects needs to be accounted for. Two cases of one row turbines at a certain wind direction are provided in Fig. 18 and Fig. 19. In the first case, WT15, WT12 and WT16 are selected, where the distances between them are 4.7 D and 5.0 D (see Fig. 18a). The observed and predicted time series of wind speed and power at the wind direction of 284° with a sector width of 5° are collected and the time-averaged values for each turbine are plotted in Fig. 18c and d. The second case is presented for WT6, WT13 and WT16, where the distances between them are 4.6 D and 5.9 D, respectively (see Fig. 19a). The observed and predicted time series of wind speed and power at the wind direction of 237° with a sector width of 5° are collected and the time-averaged values for each turbine are plotted in Fig. 19c and d. Compared with upstream turbines, the wind speed and power of downstream turbines decease due to the wake effects as shown in Figs. 18b and 19b. The predicted wind speed and power by the present wind farm flow model agree well with those obtained from SCADA data. However, the modified PARK model generally overestimates the wind speed and power especially for the third downstream turbines as shown in Figs. 18 and 19.

Finally, the power production of the whole wind farm is analyzed and the mean value and standard deviation of power output at different wind speed bins are displayed in Fig. 20. Note that the freestream wind speed at the hub height over the flat terrain without wind turbine wake effects predicted by the wind farm flow model is taken as the reference wind speed for the plot in Fig. 20. The open circles show the values obtained from SCADA data. Blue lines represent the predicted theoretical power production where the wake effects are ignored, while the predicted power production with wake effects are plotted by green lines, where the manufacture power curve is utilized. Red lines denote those predicted by using the proposed probabilistic power curve model, where the time series of power output is calculated for each wind turbine using Eq. (11). It can be seen from Fig. 20a that, with considering wake effects, the mean values of power at each wind speed bin get closer to the measurement but still underestimate those near the cut-in wind speed and overestimate those near the rated wind speed region. These discrepancies are improved by applying the proposed probabilistic power curve model to the power prediction.

To estimate the uncertainty of the power output at different wind speed, a fully dependent relationship is assumed for all turbines in the Tomamae wind farm since the area of wind farm is limited. As a result, the standard deviation of the wind farm power output can be simply estimated as follows:

$$\sigma_{P,WF} = \sum_{i=1}^{N} \sigma_{P,WT}^{i} \tag{36}$$

where N is the number of turbines, and $\sigma_{P,WT}^{i}$ is the standard deviation of individual turbine i calculated by Eq. (12). As shown in Fig. 20b, the predicted standard deviation of wind farm power production at different wind speed are well reproduced by using the proposed probabilistic

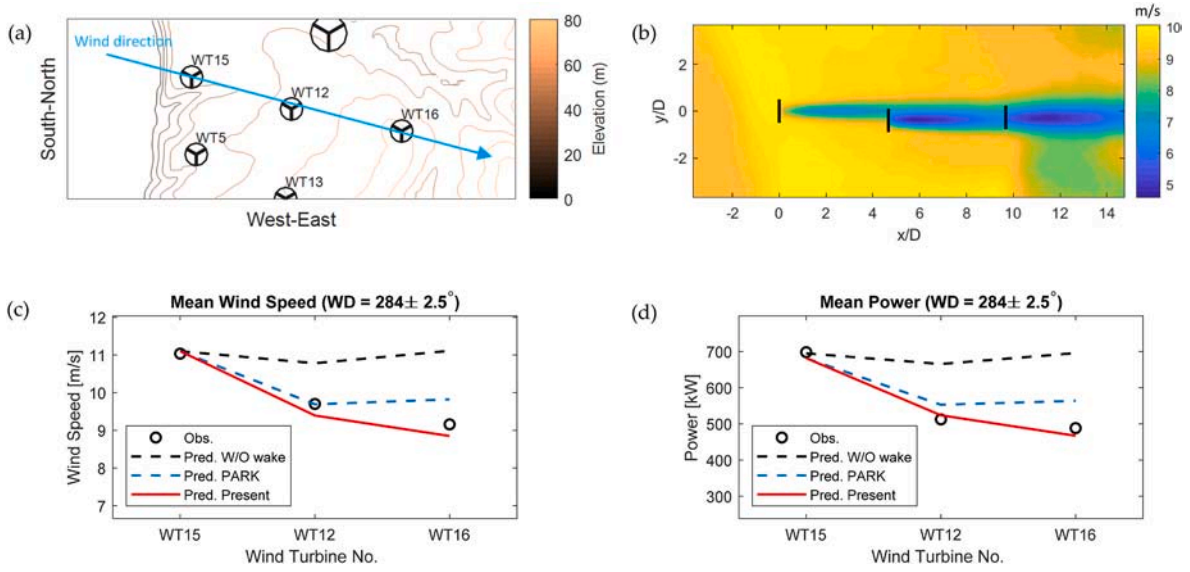

Fig. 18. Validation case of one row turbines: (a) layout of WT15, WT12 and WT16. (b) contour of mean wind speed at hub height. comparison of predicted and measured (c) wind speed and (d) power output of each turbine.

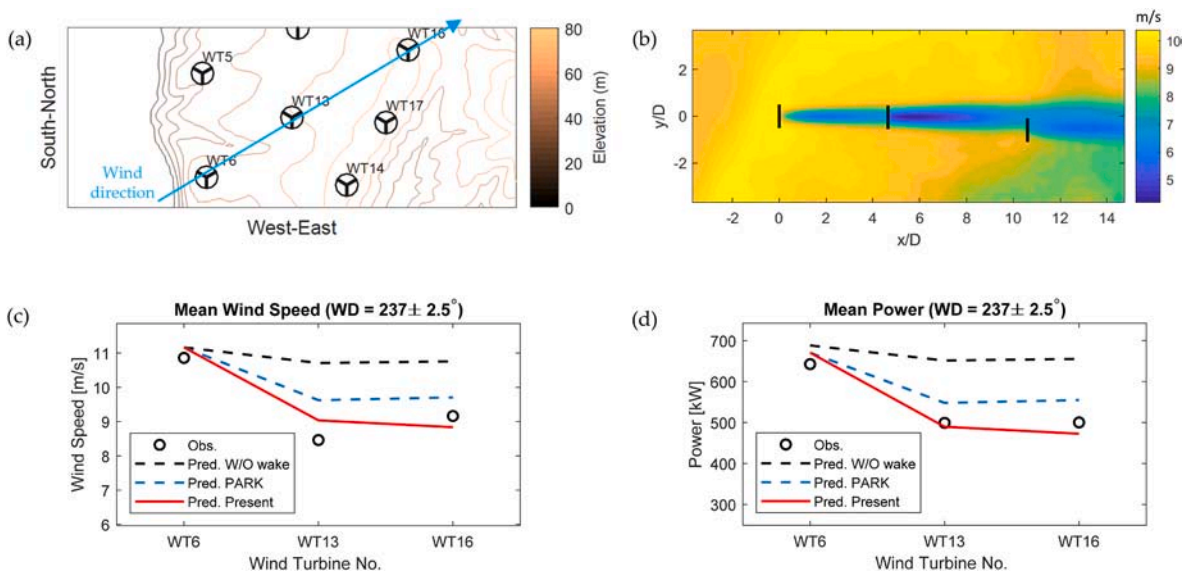

Fig. 19. Validation case of one row turbines: (a) layout of WT6, WT13 and WT16. (b) contour of mean wind speed at the hub height. comparison of predicted and measured (c) wind speed and (d) power output of each turbine.

power curve model, while the conventional manufacture power curve cannot provide the uncertainty of wind farm power production.

The weighted mean absolute percentage error in mean value and standard deviation of wind farm power are also calculated and plotted in Fig. 20c and d, respectively. As expected, the WMAPE in mean value is reduced from 18.1% to 7.2% with consideration of wake effects. Note that the prediction accuracy in mean value using the proposed probabilistic WTPC model does not provide improvement compared with the manufacture WTPC since the wind speed mainly occurs in the medium wind speed region (see Fig. 4) where the two WTPCs show almost same performance as shown in Fig. 20a. For the standard deviation, the proposed model displays much higher accuracy compared with the manufacture power curve model since the deterministic WTPC cannot predict the standard deviation in the wind farm and the WMAPE in standard deviation is reduced from 100% to 15.6% by using the proposed probabilistic WTPC.

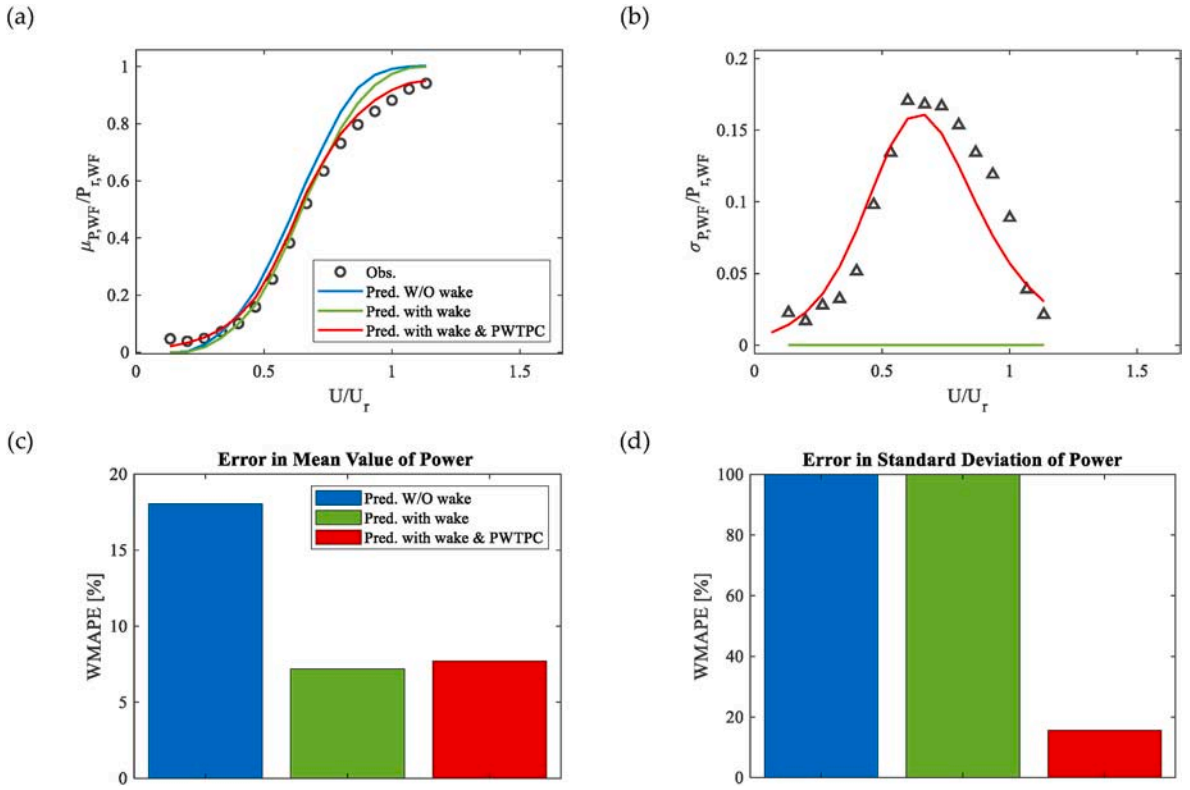

Fig. 20. Distribution of (a) mean value and (b) standard deviation of wind farm power outputs under the different normalized wind speed, as well as prediction errors in (c) mean value and (d) standard deviation. The power outputs are normalized by the rated power of wind farm $P_{r,WF}$, and the values of wind speed are normalized by the rated wind speed U_r.

4. Conclusion

In this study, a novel probabilistic power curve model is proposed and a hybrid wind farm model is presented to predict the power production for the wind farm over complex terrain. The predicted mean value and standard deviation of power production are validated by a measurement campaign conducted in the Tomamae wind farm located in the north of Japan. Following conclusions are obtained:

(1) The power production at a certain wind speed bin is modelled by the beta distribution for an active stall-controlled wind turbine based on the SCADA data analysis. The predicted mean value and standard deviation of power by the proposed probabilistic power curve model based on one wind turbine show favorable agreement with the measurements obtained from other wind turbines in the wind farm, while the normal distribution cannot accurately estimate the probability distribution of power output of wind turbine when the wind speed is lower than 6 m/s and higher than 13 m/s.
(2) A hybrid wind farm model with low computational cost for wind flow prediction over complex terrain is validated by the measured wind speed obtained from Met-masts and wind turbine SCADA. The predicted wind speed and turbulence intensity by the CFD simulation combined with the Ishihara-Qian wake model show good agreement with the measurements, while the conventional modified PARK model underestimates the turbine induced turbulence and overestimates the wind speed and power production as well.
(3) The proposed probabilistic power curve model combined with the hybrid farm flow model is validated by the measurements. The predicted mean value and standard deviation of power production in the wind farm show favorable agreement with the measurements. The weighted mean absolute percentage error in mean power production in the wind farm is reduced from 18.1% to 7.2% with consideration of wake effects and that in standard deviation is reduced from 100% to 15.6% by using the proposed probabilistic power curve model.

CRediT author statement

Guo-Wei Qian: Investigation, Software, Writing-Original draft preparation, Formal analysis, Visualization, Data Curation, and Simulation. **Takeshi Ishihara**: Resources, Conceptualization, Methodology, Supervision, Writing-Reviewing and Editing.

Declaration of competing interest

The authors declare that they have no known competing financial interests or personal relationships that could have appeared to influence the work reported in this paper.

Data availability

The data that has been used is confidential.

Acknowledgements

This research was carried out as part of a joint program funded by ClassNK, J-POWER, Shimizu Corporation, Toshiba Energy Systems & Solutions Corporation, and MHI Vestas Offshore Wind Japan. The authors would like to acknowledge New Energy and Industrial Technology Development Organization (NEDO) for providing LiDAR data and Eurus Energy Holdings Corporation for SCADA data of wind farm.

References

[1] WindFarmer. Wind farm design software: theory manual. Garrad Hassan and Partners Ltd; 2014.
[2] IEC. Iec 61400-12-1. In: International Electrotechnical Commission; 2005. p. 179. 2005.
[3] Wang Y, Hu Q, Li L, Foley AM, Srinivasan D. Approaches to wind power curve modeling: a review and discussion. Renew Sustain Energy Rev 2019;116:109422. https://doi.org/10.1016/j.rser.2019.109422.
[4] Torres JL, Prieto E, Garcia A, De Blas M, Ramirez F, De Francisco A. Effects of the model selected for the power curve on the site effectiveness and the capacity factor of a pitch regulated wind turbine. Sol Energy 2003;74:93–102. https://doi.org/10.1016/S0038-092X(03)00144-0.
[5] Diaf S, Diaf D, Belhamel M, Haddadi M, Louche A. A methodology for optimal sizing of autonomous hybrid PV/wind system. Energy Pol 2007;35:5708–18. https://doi.org/10.1016/J.ENPOL.2007.06.020.
[6] Yan J, Osadciw LA, Benson G, White E. Inverse data transformation for change detection in wind turbine diagnostics. In: Canadian Conference on Electrical and Computer Engineering; 2009. p. 944–9. https://doi.org/10.1109/CCECE.2009.5090267.
[7] Villanueva D, Feijóo AE. Reformulation of parameters of the logistic function applied to power curves of wind turbines. Elec Power Syst Res 2016;137:51–8. https://doi.org/10.1016/J.EPSR.2016.03.045.
[8] Villanueva D, Feijóo A. Comparison of logistic functions for modeling wind turbine power curves. Elec Power Syst Res 2018;155:281–8. https://doi.org/10.1016/J.EPSR.2017.10.028.
[9] Bulaevskaya V, Wharton S, Clifton A, Qualley G, Miller WO. Wind power curve modeling in complex terrain using statistical models. J Renew Sustain Energy 2015;7. https://doi.org/10.1063/1.4904430.
[10] Pandit RK, Infield D, Kolios A. Gaussian process power curve models incorporating wind turbine operational variables. Energy Rep 2020;6:1658–69. https://doi.org/10.1016/j.egyr.2020.06.018.
[11] Pelletier F, Masson C, Tahan A. Wind turbine power curve modelling using artificial neural network. Renew Energy 2016;89:207–14. https://doi.org/10.1016/j.renene.2015.11.065.
[12] Üstüntaş T, Şahin AD. Wind turbine power curve estimation based on cluster center fuzzy logic modeling. J Wind Eng Ind Aerod 2008;96:611–20. https://doi.org/10.1016/J.JWEIA.2008.02.001.
[13] Kusiak A, Zheng H, Song Z. On-line monitoring of power curves. Renew Energy 2009;34:1487–93. https://doi.org/10.1016/J.RENENE.2008.10.022.
[14] Schlechtingen M, Santos IF, Achiche S. Using data-mining approaches for wind turbine power curve monitoring: a comparative study. IEEE Trans Sustain Energy 2013;4:671–9. https://doi.org/10.1109/TSTE.2013.2241797.
[15] Stephen B, Galloway SJ, McMillan D, Hill DC, Infield DG. A copula model of wind turbine performance. IEEE Trans Power Syst 2011;26:965–6. https://doi.org/10.1109/TPWRS.2010.2073550.
[16] Wei D, Wang J, Li Z, Wang R. Wind power curve modeling with hybrid copula and grey wolf optimization; wind power curve modeling with hybrid copula and grey wolf optimization. IEEE Trans Sustain Energy 2022;13. https://doi.org/10.1109/TSTE.2021.3109044.
[17] Her S, Huh J, Kim B. Formula for estimating the uncertainty of manufacturer's power curve in pitch-controlled wind turbines. IET Renew Power Gener 2018;12:292–7. https://doi.org/10.1049/iet-rpg.2017.0081.
[18] Xu K, Yan J, Zhang Hao, Zhang Haoran, Han S, Liu Y. Quantile based probabilistic wind turbine power curve model. Appl Energy 2021;296:116913. https://doi.org/10.1016/j.apenergy.2021.116913.
[19] Yun E, Hur J. Probabilistic estimation model of power curve to enhance power output forecasting of wind generating resources. Energy 2021;223:120000. https://doi.org/10.1016/j.energy.2021.120000.
[20] Wang H, Xue W, Liu Y, Peng J, Jiang H. Probabilistic wind power forecasting based on spiking neural network. Energy 2020;196:117072. https://doi.org/10.1016/j.energy.2020.117072.
[21] Jin T, Tian Z. Uncertainty analysis for wind energy production with dynamic power curves. In: 2010 IEEE 11th international conference on probabilistic methods applied to power systems. PMAPS; 2010. p. 745–50. https://doi.org/10.1109/PMAPS.2010.5528405.
[22] Lange M, Focken U. Physical approach to short-term wind power prediction. In: Physical Approach to Short-Term Wind Power Prediction; 2006. p. 1–208. https://doi.org/10.1007/3-540-31106-8.
[23] Yan J, Zhang H, Liu Y, Han S, Li L. Uncertainty estimation for wind energy conversion by probabilistic wind turbine power curve modelling. Appl Energy 2019;239:1356–70. https://doi.org/10.1016/j.apenergy.2019.01.180.
[24] Kwon SD. Uncertainty analysis of wind energy potential assessment. Appl Energy 2010;87:856–65. https://doi.org/10.1016/j.apenergy.2009.08.038.
[25] Fleming P, King J, Bay CJ, Simley E, Mudafort R, Hamilton N, Farrell A, Martinez-Tossas L. Overview of FLORIS updates. J Phys Conf 2020;1618:022028. https://doi.org/10.1088/1742-6596/1618/2/022028.
[26] Qian GW, Ishihara T. Wind farm power maximization through wake steering with a new multiple wake model for prediction of turbulence intensity. Energy 2021;220:119680. https://doi.org/10.1016/j.energy.2020.119680.
[27] Qian GW, Ishihara T. Numerical study of wind turbine wakes over escarpments by a modified delayed detached eddy simulation. J Wind Eng Ind Aerod 2019;191:41–53. https://doi.org/10.1016/j.jweia.2019.05.004.
[28] Ansys Inc. ANSYS fluent theory guide. 2012. Canonsburg, PA.
[29] Misu Y, Ishihara T. Prediction of frequency distribution of strong crosswind in a control section for train operations by using onsite measurement and numerical

simulation. J Wind Eng Ind Aerod 2018;174:69–79. https://doi.org/10.1016/j.jweia.2017.11.020.
[30] Ishihara T, Qian G-W. A new Gaussian-based analytical wake model for wind turbines considering ambient turbulence intensities and thrust coefficient effects. J Wind Eng Ind Aerod 2018;177:275–92. https://doi.org/10.1016/j.jweia.2018.04.010.
[31] Qian G-W, Ishihara T. A new analytical wake model for yawed wind turbines. Energies 2018;11:665. https://doi.org/10.3390/en11030665.
[32] Burton T, Jenkins N, Bossanyi E, Sharpe D, Graham M. Wind energy handbook. third ed. ed. Wind Energy Handbook. Wiley; 2021. https://doi.org/10.1002/9781119992714.
[33] Aliferis AD, Jessen MS, Bracchi T, Hearst RJ. Performance and wake of a Savonius vertical-axis wind turbine under different incoming conditions. Wind Energy 2019;22:1260–73. https://doi.org/10.1002/WE.2358.
[34] Karamichailidou D, Kaloutsa V, Alexandridis A. Wind turbine power curve modeling using radial basis function neural networks and tabu search. Renew Energy 2021;163:2137–52. https://doi.org/10.1016/j.renene.2020.10.020.
[35] Martin CMS, Lundquist JK, Clifton A, Poulos GS, Schreck SJ. Wind turbine power production and annual energy production depend on atmospheric stability and turbulence. Wind Energy Sci. 2016;1:221–36. https://doi.org/10.5194/wes-1-221-2016.
[36] Geospatial information authority of Japan. 2018. http://www.gsi.go.jp/ENGLISH/index.html [WWW Document]. URL, https://fgd.gsi.go.jp/download/ref_dem.html.
[37] Enoki K, Ishihara T. A generalized canopy model and its application to the prediction of urban wind climate (in Japanese). J. Japan Soc. Civil Eng. 2012;68:28–47.
[38] MLIT [WWW Document], http://nlftp.mlit.go.jp/ksj-e/index.html; 2014.
[39] Ishihara T, Qian GW, Qi YH. Numerical study of turbulent flow fields in urban areas using modified k−ε model and large eddy simulation. J Wind Eng Ind Aerod 2020;206. https://doi.org/10.1016/j.jweia.2020.104333.